Sensors and Materials, Vol. 18, No. 3 (2006) 151–160
MYU Tokyo

S & M 0639

Improving Bias Stability of Micromachined Accelerometer by Increasing Mechanical Stability

Hyoung-Kyoon Jung*, Woon-Tahk Sung, Hyun-Kee Chang[1],
Jang Gyu Lee and Yong-Kweon Kim

School of Electrical Engineering and Computer Science, Seoul National University,
Kwanak, P.O. Box 34, Son 56-1, Silim-dong, Gwanak-gu, Seoul, Korea, 151-600

[1]Intellimicrons Co. Ltd., 8F2 60-18 Gasan-Dong Geumcheon-Gu Seoul, Korea, 153-801

(Received February 27, 2006; accepted April 3, 2006)

Key words: bias stability, mechanical stability, SiOG, high aspect ratio, micromachined accelerometer

In this paper, the bias stability of a micromachined accelerometer is improved by increasing the mechanical stability. The mechanical stability is increased by increasing the stiffness of the parallel plate electrodes of the accelerometer structure. Through this work, we experimentally show that there is a relationship between the bias stability and the mechanical stability of the accelerometer structure. We designed and fabricated two models with different mechanical stabilities. The two models of the accelerometer were designed by ANSYS modal analysis and MATLAB analysis. Silicon on glass (SiOG) substrate is used in the proposed accelerometers. Therefore, the single-crystalline silicon was used as a device layer and the glass wafer was used as a handling layer. The measured bias stability of the fabricated accelerometers was improved from 500 mg to 4.4 mg with the same sensing circuit.

1. Introduction

Inertial sensors are devices that convert an inertial force into a linearly scaled electrical signal with a given sensitivity. Until now, many inertial sensors have been developed and commercialized using various technologies. Micromachined inertial sensors, consisting of accelerometers and gyroscopes, are one of the most important types of silicon-based sensors. Microaccelerometers alone have the second-largest scaled volume after pressure sensors.[(1)] Capacitive microaccelerometers have several advantages, such as high sensitivity, low noise, stable DC characteristics, low drift, low power dissipation and low temperature sensitivity.[(2)] Recently, there have been many efforts to improve the bias stability of micromachined sensors in many sensor applications, since the practical resolution of a sensor is limited by the bias stability of the sensor. Until now, there has been much research on increasing the performance of sensors using a compensation circuit .[(3)] O'Brien et al.

*Corresponding author, e-mail address: kenjugy0@sun.ac.kr

reported that, using the outer framework, the lateral and vertical spring constants of an interdigitated capacitive accelerometer sense array can be increased, and improved resistance to process and in-use stiction can be obtained.[4] However, they could not show an improved performance of the sensor through increasing the mechanical stability. In general, the bias stability of a capacitive-sensing-type inertial sensor is largely dependent on the variance of the initial capacitance and the change in resonant frequency. As a static accelerometer is used in this study, the variance of the initial capacitance has a great effect on the bias stability error. Therefore, it is a key technology to decrease the variance of the initial capacitance of the sensor structure by increasing the mechanical stability of the micromachined structure in this study.

2. Design of Accelerometer as Test Structure

2.1 *Dynamics consideration*

In micromechanical accelerometers, a proof mass is suspended onto a substrate via a compliant suspension with a spring constant. When the substrate undergoes acceleration, the proof mass exerts a force on the suspension. For frequencies below the mechanical resonance of the spring-mass system, these forces cause the suspension to deflect a distance given by

$$x = \frac{F}{k} = \frac{m}{k}a = \frac{1}{\omega_0^2}a. \tag{1}$$

Equation (1) shows that the scale factor depends only on the resonant frequency and is not affected by the choice of a large mass and a stiff spring or a small mass and a compliant spring. In this paper, we use parallel plate electrodes as sensing electrodes. After some linearization, the change in capacitance can be expressed by

$$\Delta C \cong \frac{2C_0}{d}x, \tag{2}$$

where C_0 is the initial capacitance and d is the initial gap between the electrodes and x is a displacement. From eqs. (1) and (2), we can obtain the relationship between resonant frequency and change in capacitance when acceleration is fixed.

Figure 1 shows the relationship between resonant frequency and change in capacitance. As shown in Fig. 1, the lower the resonant frequency of the accelerometer, the larger the change in capacitance, since the displacement of the accelerometer is proportional to $\frac{1}{w_0^2}a$. Therefore, it is necessary to increase the sensitivity of the high-resonant-frequency

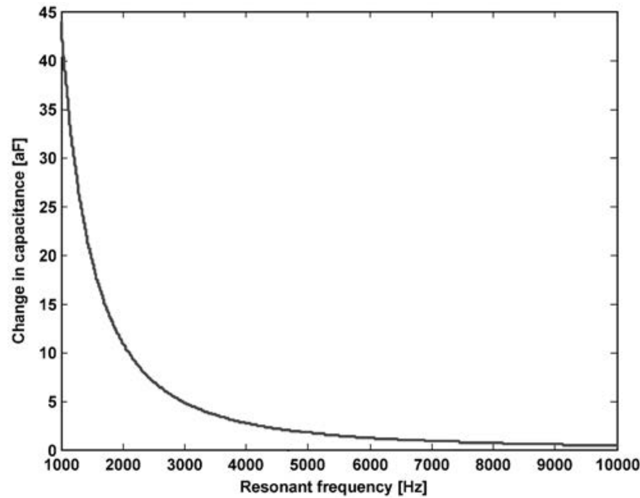

Fig. 1. Relationship between resonant frequency and change in capacitance.

accelerometer with high-aspect-ratio parallel plate electrodes.

2.2 *Design of structure*

As described in Fig. 2, the proposed device has high-aspect-ratio single-crystalline silicon structures, such as a proof mass, parallel plate electrodes and springs. Even though comb electrodes have a good linearity in large displacement, parallel plate electrodes are used in this accelerometer to increase the sensitivity of the device. As the spring constant is large for a high resonant frequency, the displacement of the accelerometer is small. Since the linearity of parallel plate electrodes is not so poor for a small displacement, the desired sensitivity and good linearity are obtained using the parallel plate electrodes. The operation principle of this accelerometer is simple. When an external acceleration is applied to the proof mass of the accelerometer, the proof mass moves along the direction of acceleration. Then the gap between the parallel plates is changed, the acceleration can be sensed through a change in capacitance. With the rebalancing electrode, a force balance technique can be adopted and we can also apply the external force to test electrodes.

Figure 3 shows the relationship between the length of proof mass and the length of spring with a 6 kHz resonant frequency. With this relationship, we select three points in Fig. 3, and then ANSYS simulation is performed to find the optimum structural dimension of the proposed accelerometer. Simplified models are used for the simulation. The etch-hole and parallel plate electrodes are omitted in structure modeling, but those are considered to be due to the density of the proof mass.

Figure 4 shows the first mode and the second mode characteristics of the accelerometer of model 1. The first mode is translation motion and the second mode is a bending motion of the proof mass. Table 1 represents the results of the ANSYS simulation of the three selected points, where f_{r1}, f_{r2}, f_{r2}/f_{r1} and W_P are the resonant frequency of the first mode, the

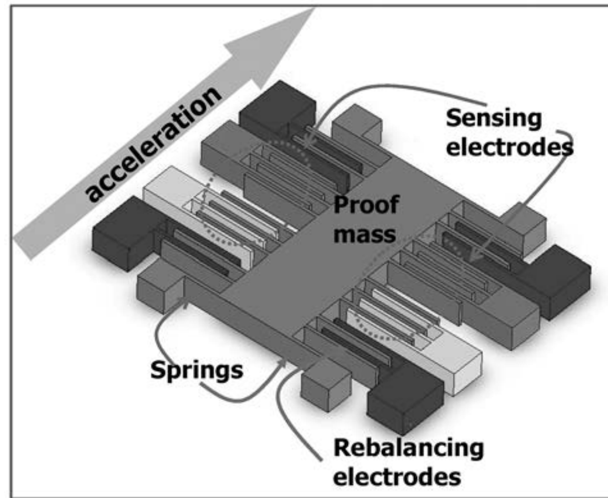

Fig. 2. Schematics of proposed accelerometer.

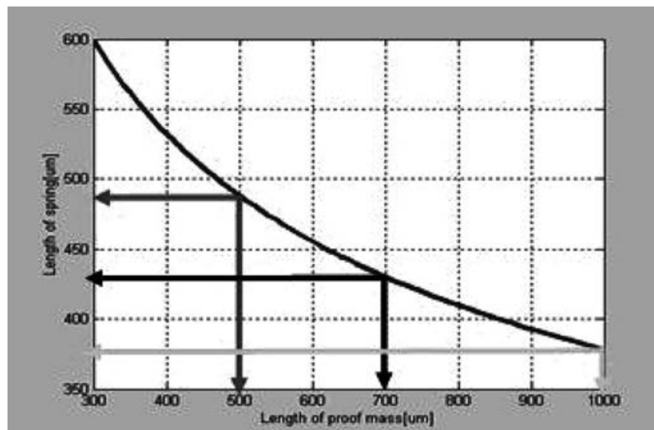

Fig. 3. Relationship of length of proof mass and length of spring.

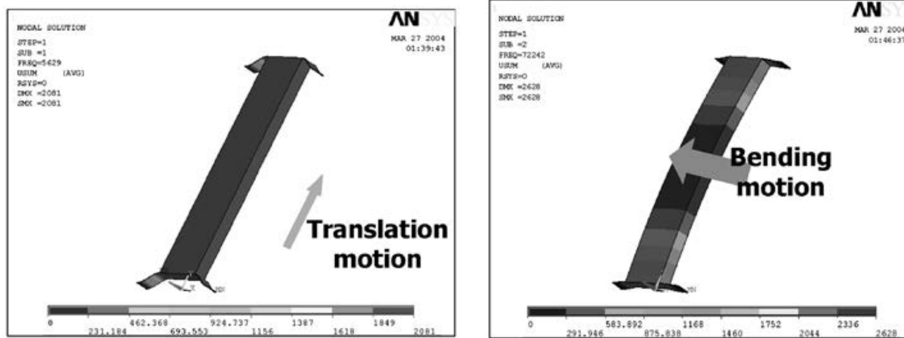

(a) First mode: 5629 Hz

(b) Second mode: 72242 Hz

Fig. 4. Results of ANSYS simulation of model 1.

Table 1
ANSYS simulation result.

W_p (μm)	f_{r1} (Hz)	f_{r2} (Hz)	f_{r2}/f_{r1}
500	5629	72242	12.83
700	5739	70667	12.31
1000	5808	67698	11.66

resonant frequency of the second mode, the ratio of the resonant frequencies of the first and second modes and the length of proof mass, respectively. As shown in Table 1, f_{r2}/f_{r1} is largest when W_P is 500 μm. This means that the structure is strong in the direction of the second mode. Therefore, a low off-axis sensitivity is expected in the proposed accelerometer. From these simulation results, W_P is set to 500 μm.

Figure 5 shows the mode characteristics of the proposed accelerometer of model 2, when the length of proof mass is 500 μm. The mode sequences of model 2 are similar to the mode sequences of model 1, and the first mode and second mode resonant frequencies of model 2 are 3270 and 37513 Hz, respectively. Therefore, the ratio of the first mode and second mode frequencies is calculated to be 11.48.

As shown in Figs. 4 and 5, the mode characteristics of the two models are almost the same. Because simplified models are used for the simulation, we can show that the mechanical characteristics of the two models, except for parallel plate electrodes, is almost the same.

2.3 *Parameter calculation*

To increase mechanical stability there are two differences between the first and second models. The first difference is the stiffness change of the parallel plate electrodes of the sensor, and the second difference is the pattern change for a more accurate structure definition.

The resonant frequency of model 1 is designed to be 6 kHz, and that of the model 2 is designed to be 3.2 kHz, and the length, width and thickness of the electrode are different between the two models. The differences between the first and second models are summarized in Table 2.

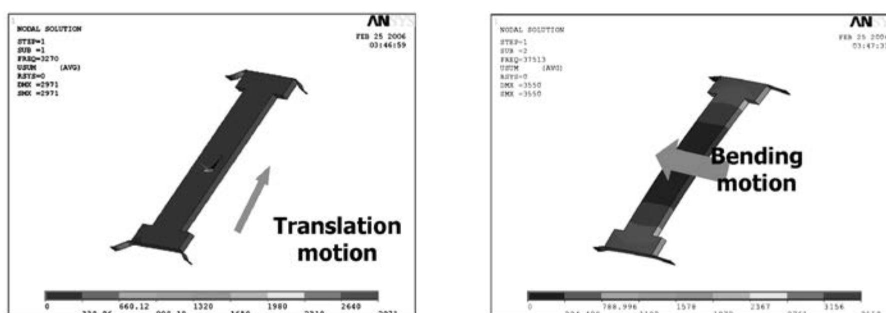

(a) First mode: 3270 Hz (b) Second mode: 37513 Hz

Fig. 5. Results of the ANSYS simulation of model 2.

Table 2
Differences between two models

	Resonant frequency	Mass	Q-factor	Equivalent acceleration noise	Electrode length	Electrode width	Stiffness of electrode	Electrode pair
unit	(Hz)	(kg)	–	(μg)	(μm)	(μm)	(N/m)	–
Model 1	6000	2.31×10^{-7}	0.02	37.1	400	4	2.81	50
Model 2	3200	1.75×10^{-7}	0.09	14.6	300	6	16	60

The mean-square equivalent acceleration noise is derived as[5]

$$a_{\mathrm{n,rms}} = \sqrt{\frac{4k_{\mathrm{B}}T\omega_0}{mQ}}, \tag{3}$$

where k_{B} is the Boltzmann constant, T is the absolute temperature, ω_0 is the resonant frequency, m is the proof mass, and Q is the quality factor of the sensor.

3. Fabrication

The proposed accelerometer is fabricated by a single mask process, which uses a silicon-glass anodic bonded wafer.[6] Because the accelerometer structure has only one structure layer, the fabrication process of the device is simple. Figure 6 shows the fabrication process.

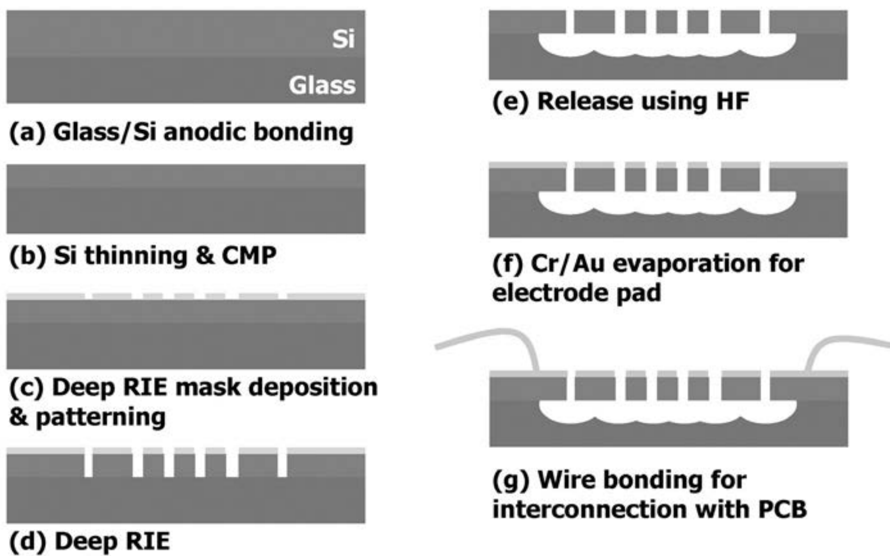

Fig. 6. Fabrication process.

The process begins with the anodic bonding of a single crystalline wafer and a Pyrex #7740 glass wafer. The bonded wafer is chemically etched in KOH solution and polished by chemical mechanical polishing (CMP) to obtain a 100-μm-thick device. The polishing is followed by silicon dioxide deposition on the silicon surface as a deep RIE mask. Then, the pattern of the accelerometer is defined on the silicon dioxide surface by photolithography, and the single-crystalline silicon is etched by deep RIE. The structure is released by glass etching in HF solution. The etching is followed by Cr/Au evaporation on the silicon surface for the formation of electrodes. Finally, wire bonding with PCB is performed.

Figures 7 and 8 show the fabricated results. Figures 7(a) and 7(b) are SEM images of the fabricated micromachined accelerometer. Figures 8(a) and 8(b) are enlarged views of the electrodes of the two models. As can be seen in Fig. 8, the differences between the two models are round-ended springs and circle-type etch-holes. The mismatch of the suspension springs caused by fabrication error is reduced with a round-ended spring and circle-type etch-holes because a convex or concave corner with a right angle cannot be fabricated exactly.

4. Measurement

The bias stabilities of the two models were measured. Bias stability is an output when no acceleration is applied, and is calculated from the turn-on time of the system. From the turn-on time, we obtain the output of the accelerometer when no acceleration is applied, and the value of the bias stability is obtained by calculating the standard deviation of the sensor output for 60 min. The measured value of the bias stability is 500 mg for model 1 and 4.4 mg for model 2. Figure 9 represents the measurement results of bias stability. This result will be considered in the discussion section. It is experimentally shown that bias stability can be improved by increasing mechanical stability.

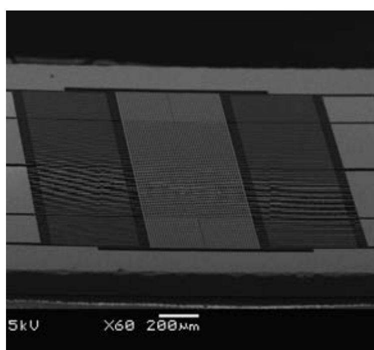

(a) Model 1

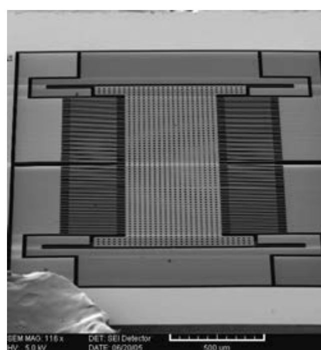

(b) Model 2

Fig. 7. SEM images of fabricated accelerometer.

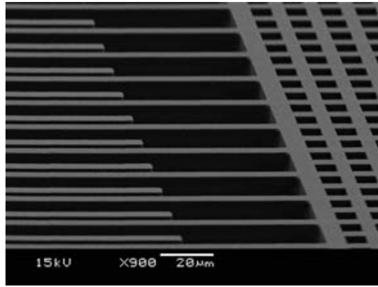

(a) Model 1

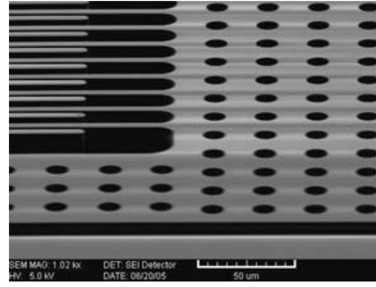

(b) Model 2

Fig. 8. SEM images of fabricated structures of the models 1 and 2.

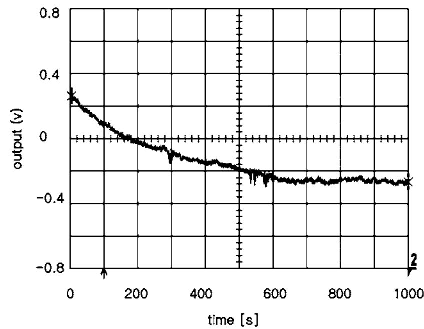

(a) Model 1: 500 mg

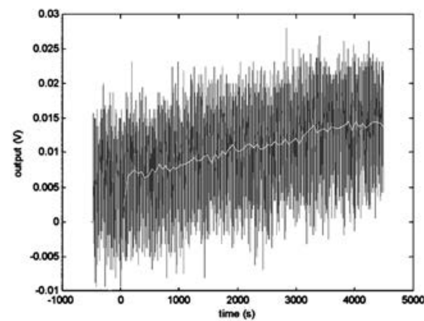

(b) Model 2: 4.4 mg

Fig. 9. Measured bias stabilities of two accelerometer models from turn-on time.

5. Discussion

The micromachined accelerometer is designed, fabricated and measured to show the relationship between the bias stability and the mechanical stability of the accelerometer structure. Model 2 has greater bias stability than model 1. However, model 2 only has 2.5 times lower mean-square equivalent acceleration noise than model 1. The stiffness of the parallel plate electrodes of models 1 and 2 are 2.81 and 16 N/m, respectively. The stiffness of the electrodes of model 2 is 5.7 times larger than that of model 1, and the numbers of electrode pairs of the two models are 50 and 60, respectively. The mechanical instability of the parallel plate electrodes is amplified by the number of electrode pairs. The bias stability

of model 2 is greater than that of model 1. The measured bias stability of the fabricated accelerometers is improved from 500 mg to 4.4 mg by increasing the mechanical stability of the accelerometer structure. Since the same sensing circuit is used, the increasing of the mechanical stability of the parallel plate electrodes can explain the excellent improvement of the bias stability. Through this work, we can show that the mechanical stability of the accelerometer structure has a great role in the bias stability of the static accelerometer. It is expected that the results of this paper can be applied to the application of the capacitive-sensing-type inertial sensor.

Acknowledgement

This work was supported by Ministry of Information and Communication Republic of Korea under the Development of 3D Smart Input Device project.

References

1 N. Yazdi, F. Ayazi and K. Najafi: Proc. IEEE (1998) p. 1640.
2 J. Chae, H. Kulah and K. Najafi: J. Microelectromech. Syst. **13** (2004) 628.
3 A. Kourepenis, J. Borenstein, J. Connelly, R. Elliott, P. Ward and M. Weinberg: Proc. AIAA GN&C Conf. 1998 (IEEE, Palm Springs, 1998) p. 1307.
4 G. J. O’□Brien, J. Hammond, G. Li, D. Koury and D. J. Monk: TechDig. 13th Int. Conf. On Solid-State Sensors and Actuators 2005 (IEEE, Seoul, 2005) p. 176.
5 S. D. Senturia: Microsystem Design (Kluwer Academic Publishers, Boston, 2001) Chap. 19.
6 C-.H. Kim and Y.-K. Kim: J. Micromech. Microeng. **12** (2002) 103.